

Systèmes de référence célestes

P. Charlot

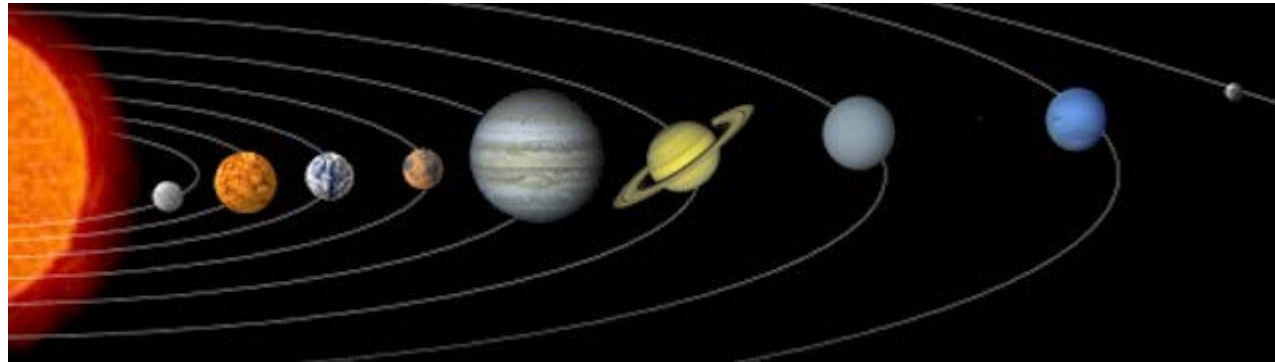
Laboratoire d'Astrophysique de Bordeaux



Outline

- **Introduction**
 - Dynamical and kinematical reference frames
 - Mach's principle
- **The extragalactic frame**
 - The sources
 - Initial VLBI realizations: ICRF and ICRF2
 - Optical realization: Gaia-CRF2
- **The new VLBI realization: ICRF3**
 - Data sets
 - Analysis configuration and properties of the frame
 - Comparison with ICRF2 and Gaia-CRF2
- **Applications of the ICRF**
 - Differential astrometry
 - Earth's rotation
 - Geophysics

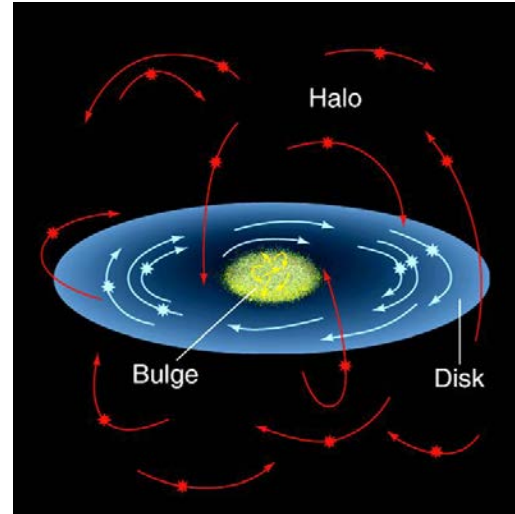
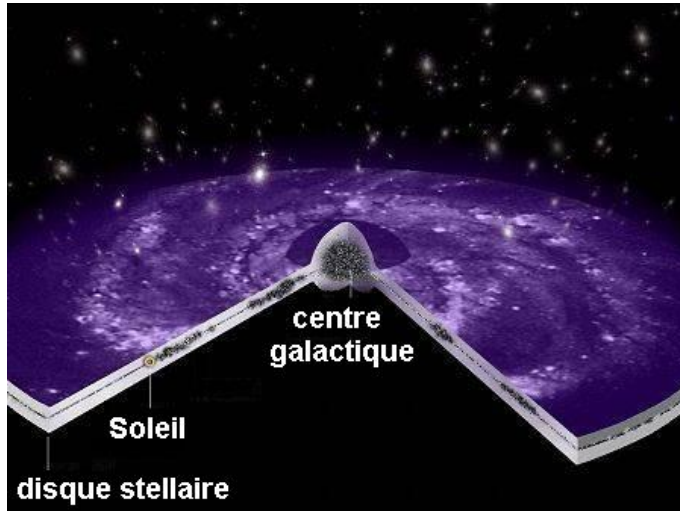
The Solar system dynamical frame



Credit: GCSE Astronomy

- Type: « dynamical » (i.e. defined by the law of dynamics)
- In practice: is defined by the inertial coordinate system in which the equations of motion of the Solar system bodies are integrated
- Access: through of the ephemerides of planets and other bodies in the Solar system

The stellar frame

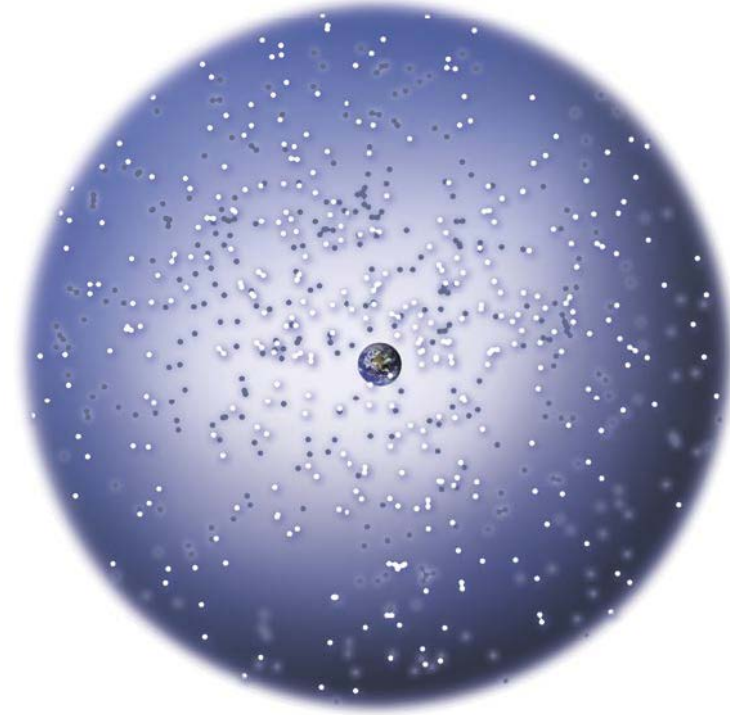


- Defined by the positions and proper motions of stars in the Galaxy
- Type: « kinematical », i.e. non-rotating with respect to a local inertial frame
- Has a reference epoch attached (B1950, J2000)
- Fundamental frame of the IAU until 1997. The latest version, the FK5, comprised 1535 stars brighter than $M_v = 7.5$

The extragalactic frame

- Type: « kinematical », i.e. non-rotating with respect to a local inertial frame
- Defined by directions of extragalactic sources (quasars) observed initially by VLBI and more recently by Gaia
- Objects located at cosmological distances, hence without proper motions
- Adopted in 1998 as fundamental frame by IAU, replacing the FK5 stellar frame

The quasar « sphere » around the Earth



Credit: IVS

Equivalence between dynamical and kinematical frames

- In 19th century, Mach was struck by the agreement between the rotation speed of the Earth measured by Foucault's pendulum (local experiment) and that measured with respect to distant stars (global experiment).
- To explain it, he invoked a causal relationship between the inertial properties of the local frame and the distant stars → Mach's principle: the inertia of a body is driven by its interaction with all matter in the Universe.
- Modern « reduced » principle: there is a particular reference frame in which distant galaxies have an isotropic recession motion with respect to any point in the Universe; in that frame, matter has neither global rotation, nor regional deformation (rotation)
→ Mach's principle implies the absence of rotation of the Universe (i.e. of rotation between a local dynamical frame and the extragalactique frame).

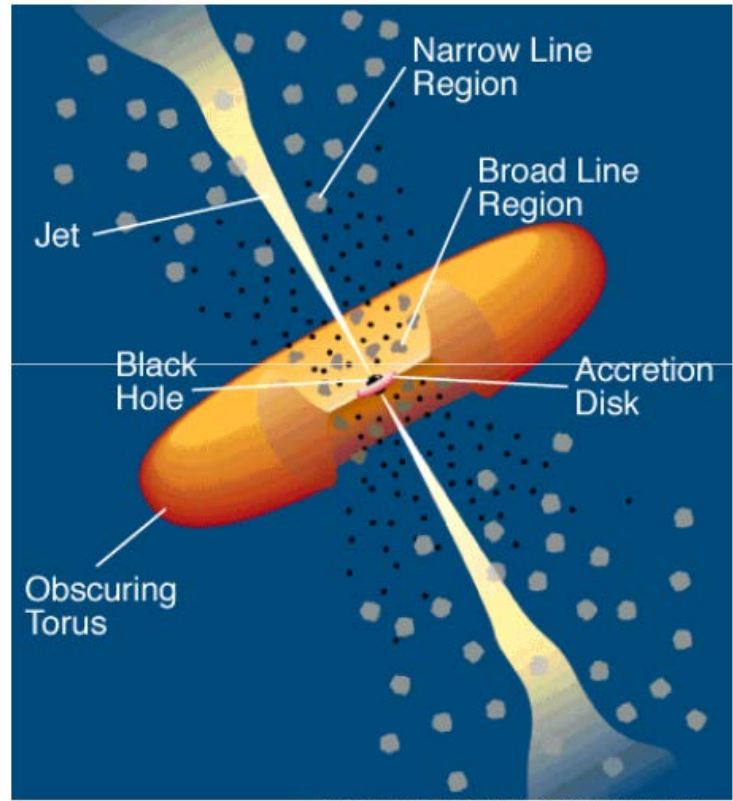
The extragalactic frame

The quasars

Major AGN components

- Black hole
- Accretion disk
- Torus
- Pair of relativistic jets

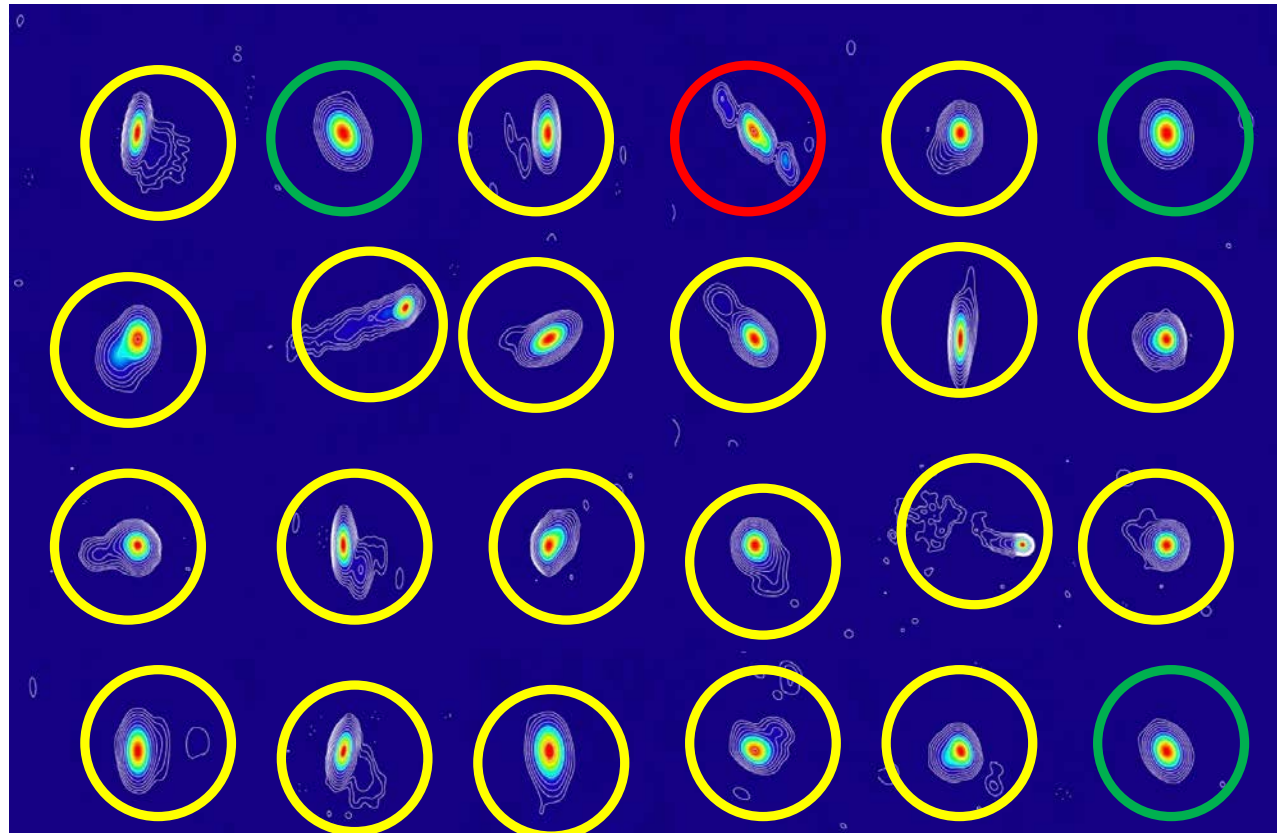
AGN standard unified model



http://heasarc.gsfc.nasa.gov/docs/objects/agn/agn_model.html

Credit: C.M. Urry & P. Padovani

Source morphology in radio



 Point-like

 One sided

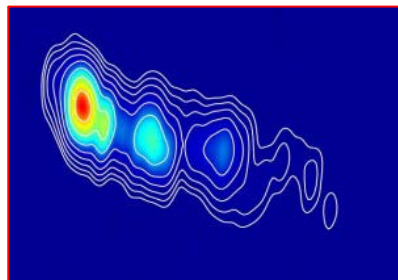
 Two-sided

A sample of X band (8 GHz) VLBI maps with milliarcsecond resolution picked up randomly from the *Bordeaux VLBI Image Database (BVID)*

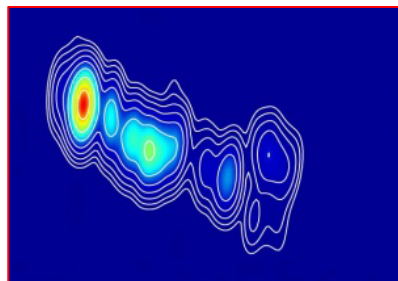
Time evolution

3C120

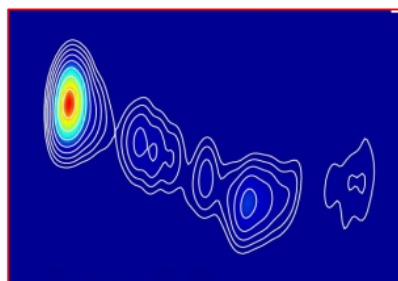
2000



2001

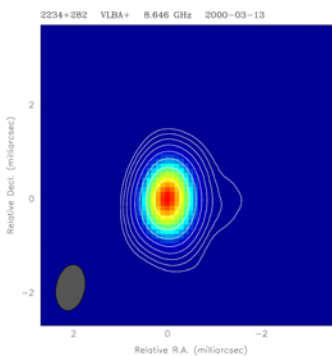


2003

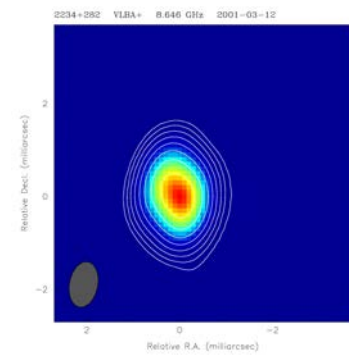


2234+282

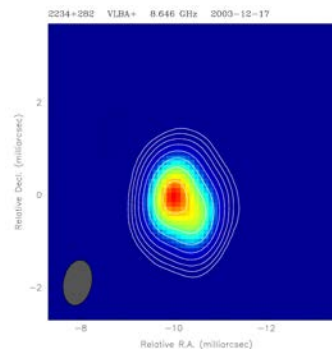
2000



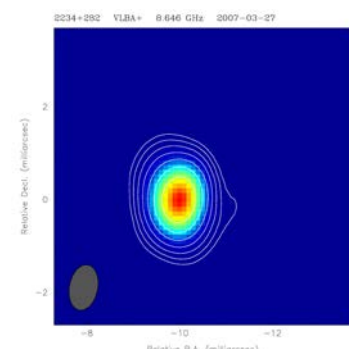
2001



2003

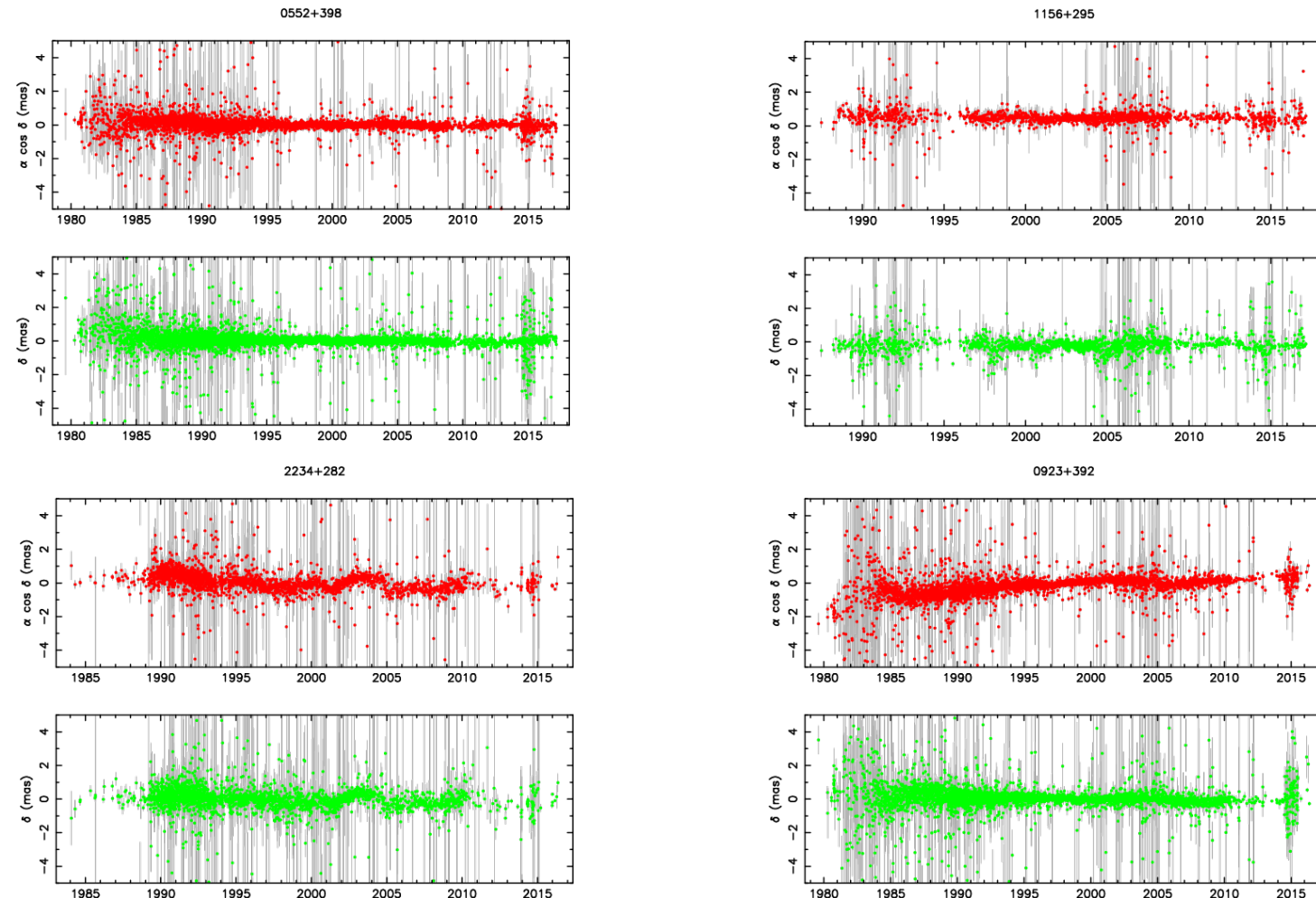


2007



Credit:
Bordeaux VLBI
Image Database

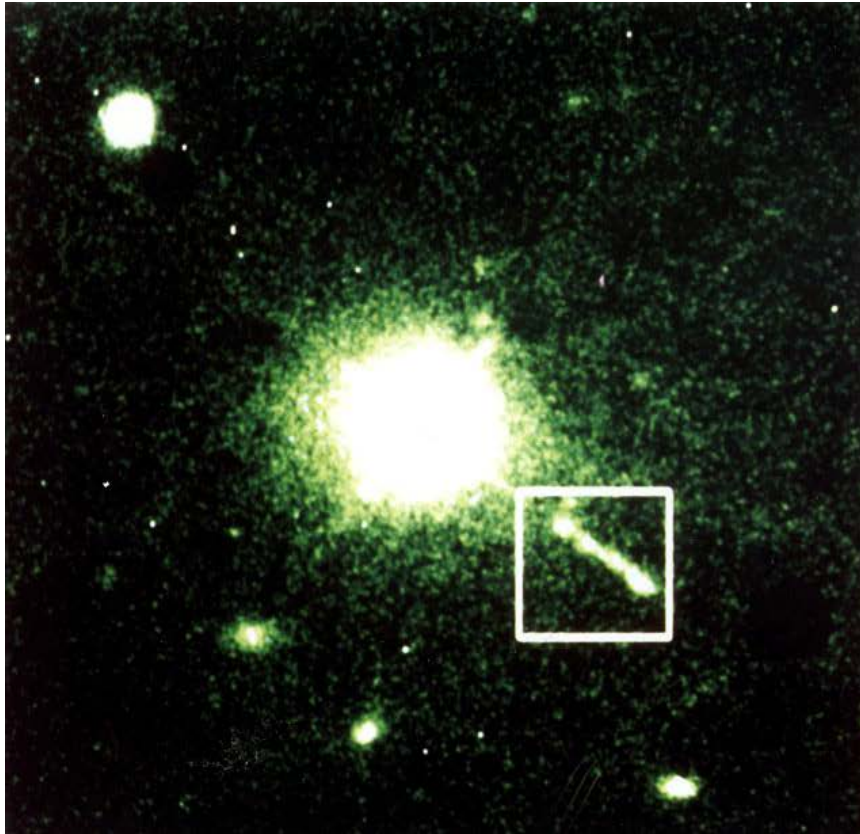
Source position stability



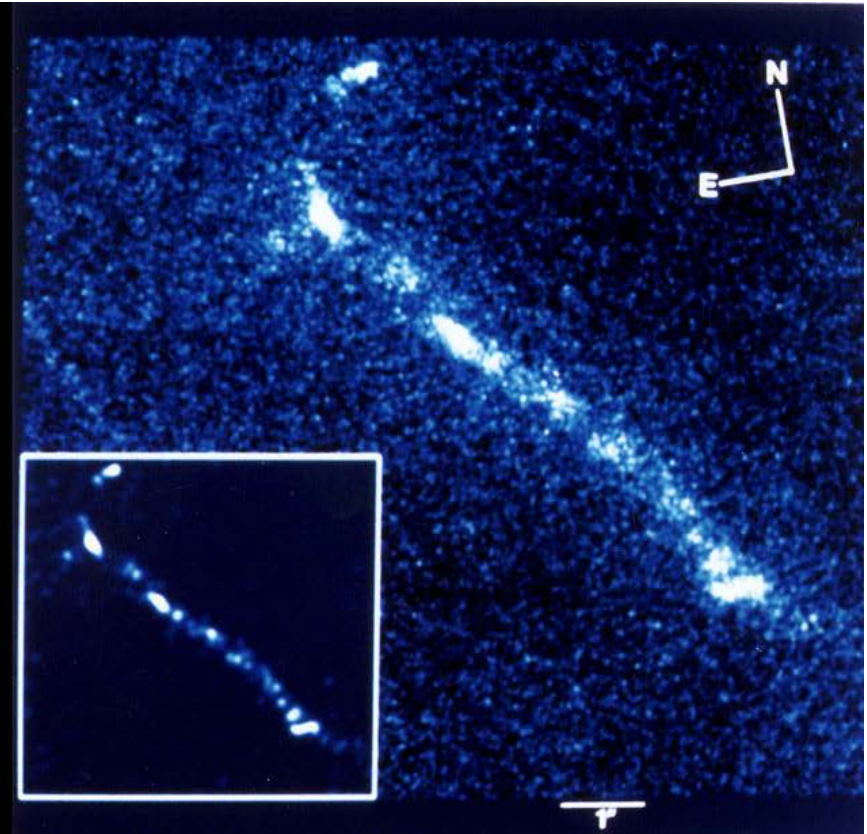
Figures courtesy of OPAR IVS Analysis Center

Optical jets do exist too...

3C273



HST observations

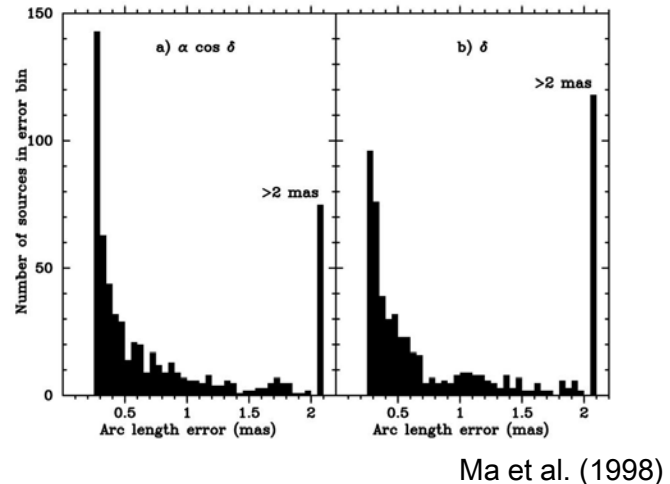
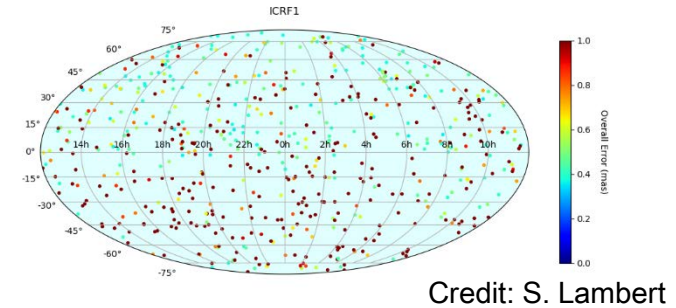


Credit: R.C. Thomson, IoA, Cambridge, UK; C.D. Mackay, IoA, Cambridge, UK; A.E. Wright, ATNF, Parkes, Australia

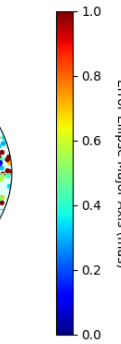
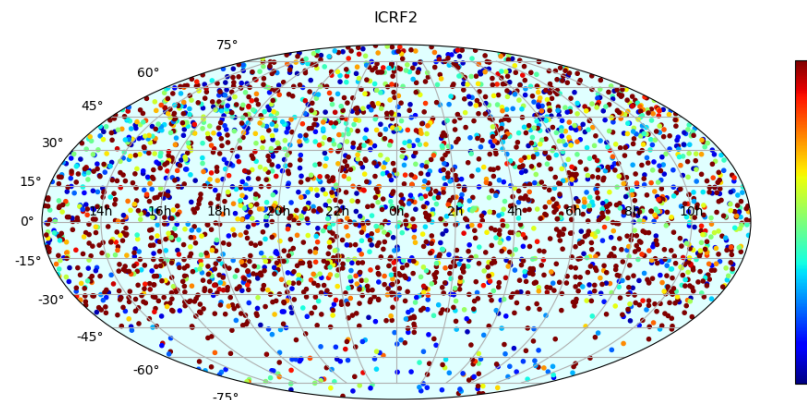
The ICRF

ICRF=International Celestial Reference Frame

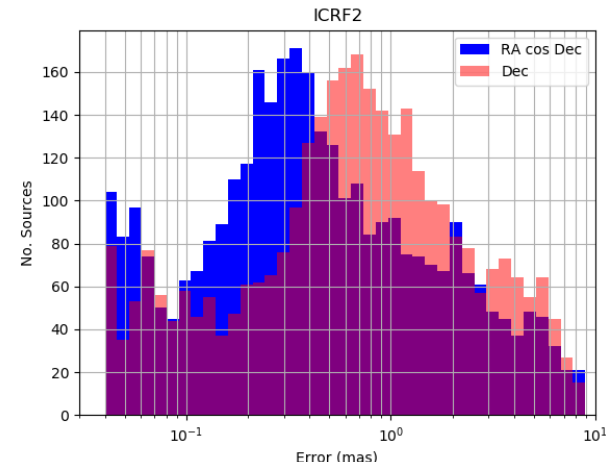
- Based on extragalactic radio sources (quasars) observed with VLBI
- 1.6 million observations acquired at dual-frequency X/S band (8.4/2.3 GHz) between 1979 to 1995
- ICRF key features
 - 608 sources in total
 - covering the entire sky
 - 212 defining sources
 - Noise floor: 250 μ as
- Adopted as IAU fundamental frame in 1998, replacing the FK5
- Extensions 1 & 2 added another 109 sources to ICRF in 2004



ICRF2



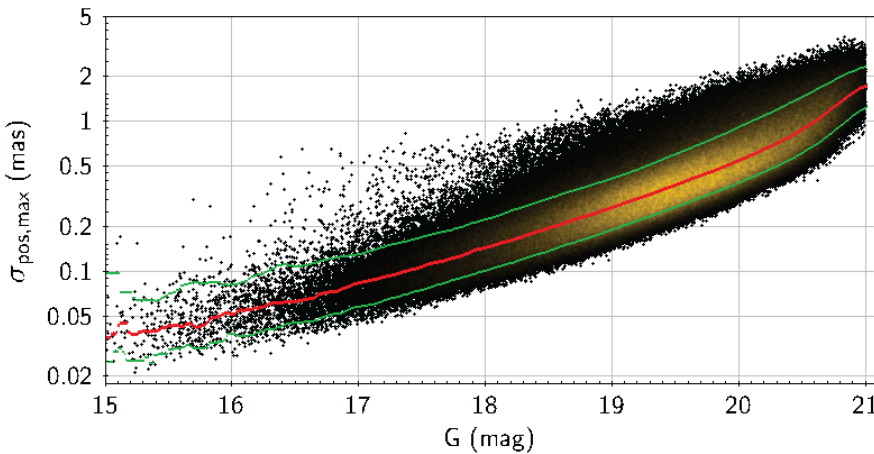
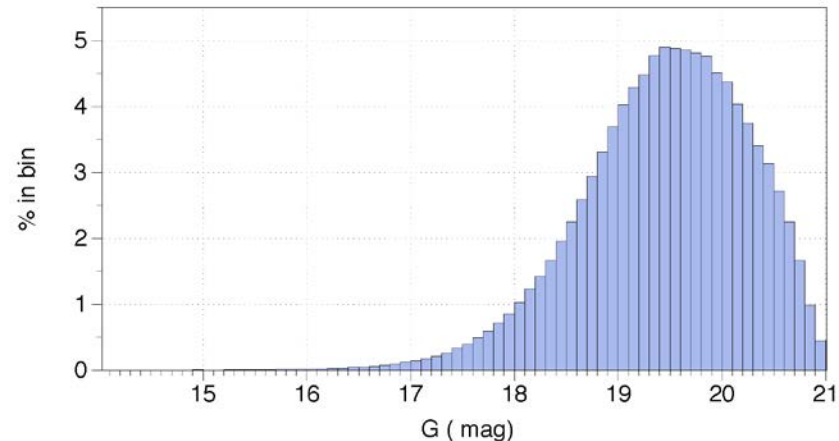
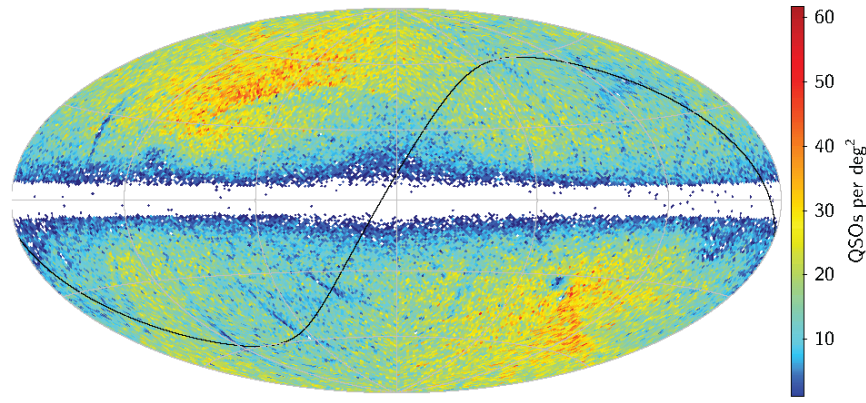
Credit: S. Lambert



- ICRF2 built in 2009, adding another 14 years of data (1995-2009), for a total of 6.5 millions observations
- Adopted by IAU at XXVIIth General Assembly (Rio de Janeiro, 2009)
- Has 3414 sources, of which 295 are defining sources
- Noise floor in individual source coordinates: 40 μ as
- About 2/3 of the sources result from single-epoch survey observations and have much lower position accuracy

Gaia-CRF2 (Data Release 2)

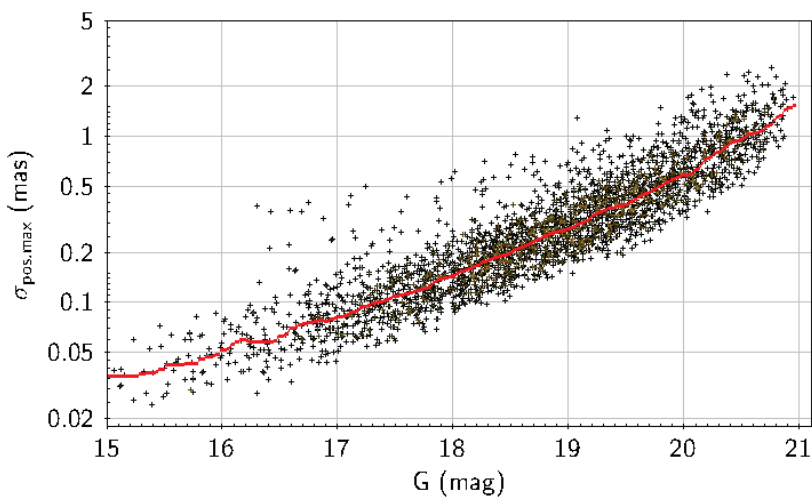
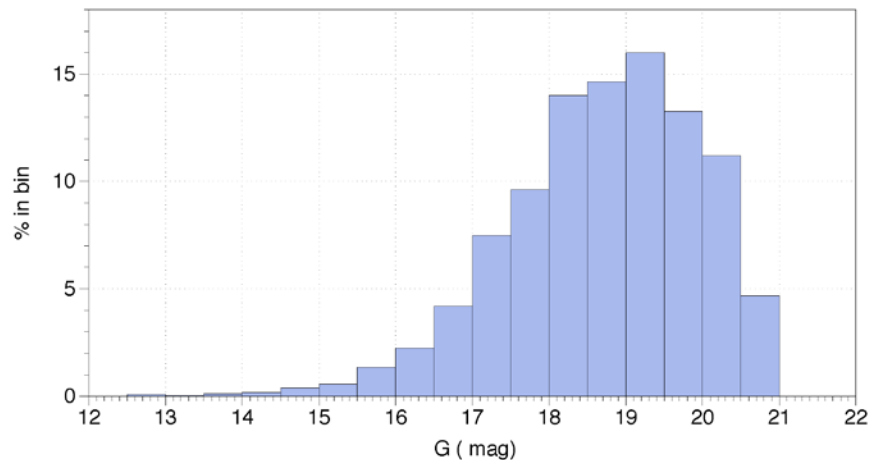
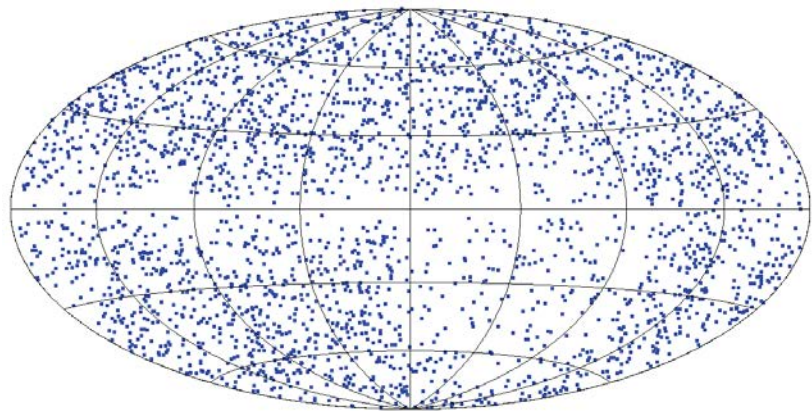
556 869 sources



25 April 2018

Mignard et al. (2018)

Gaia-CRF2 sources in ICRF3 prototype

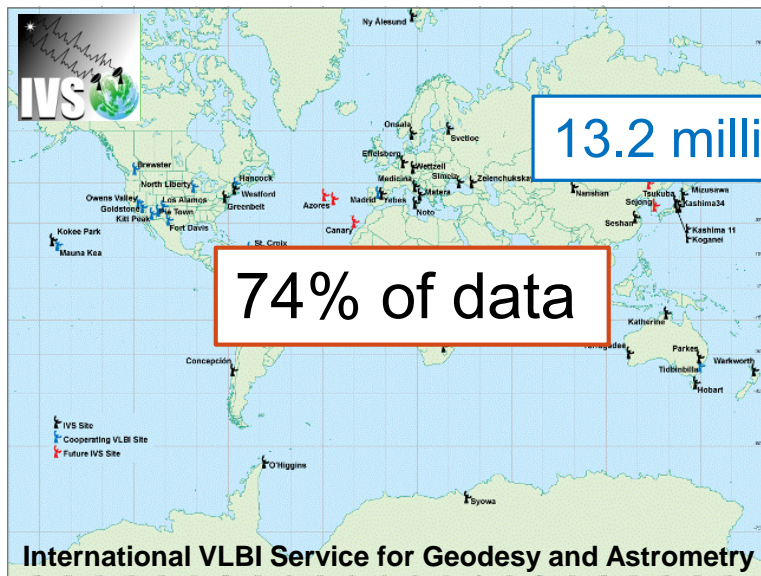


2820 common sources

Mignard et al. (2018)

The new VLBI realization: ICRF3

Data sets: S/X band (2.3/8.4 GHz)



74% of data

13.2 million observations

Very Long Baseline Array (VLBA)

26% of data

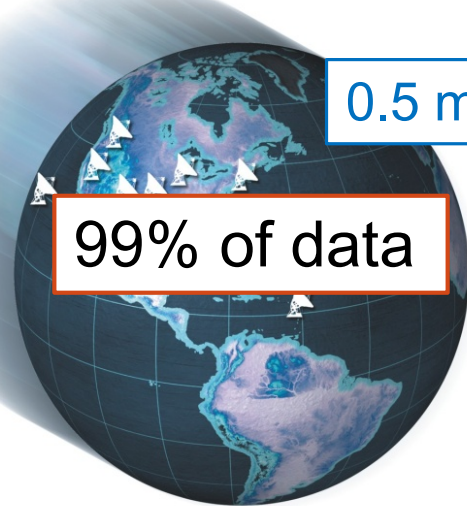
Exclusive observations
for ~2/3 of the sources

- 6206 sessions incorporating 2 to 20 IVS telescopes (1979-2018)
- 128 sessions also incorporating the 10 VLBA telescopes
- 24 VCS-I sessions* (1994-2007)
- 8 VCS-II sessions (2014-2015)
- 24 additional VCS-type sessions under USNO time (2017-2018)

* VCS=VLBA Calibrator Survey

Data sets: K band (24 GHz)

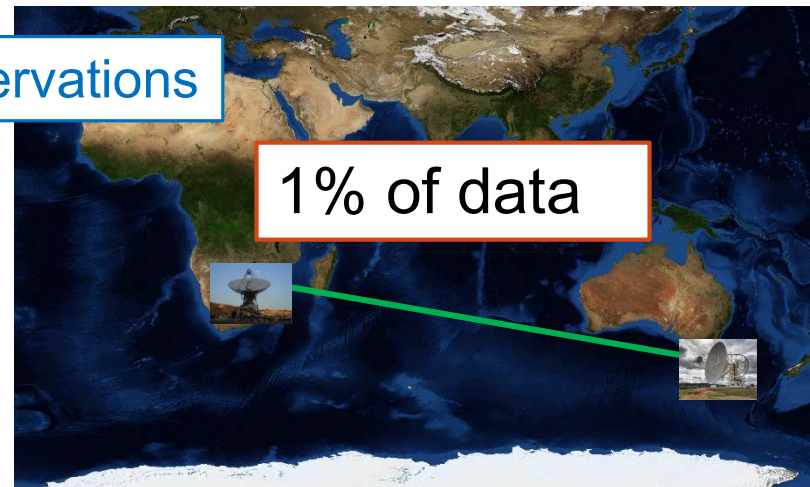
Very Long Baseline Array (VLBA)



99% of data

0.5 million observations

Hartebeesthoek-Hobart observations

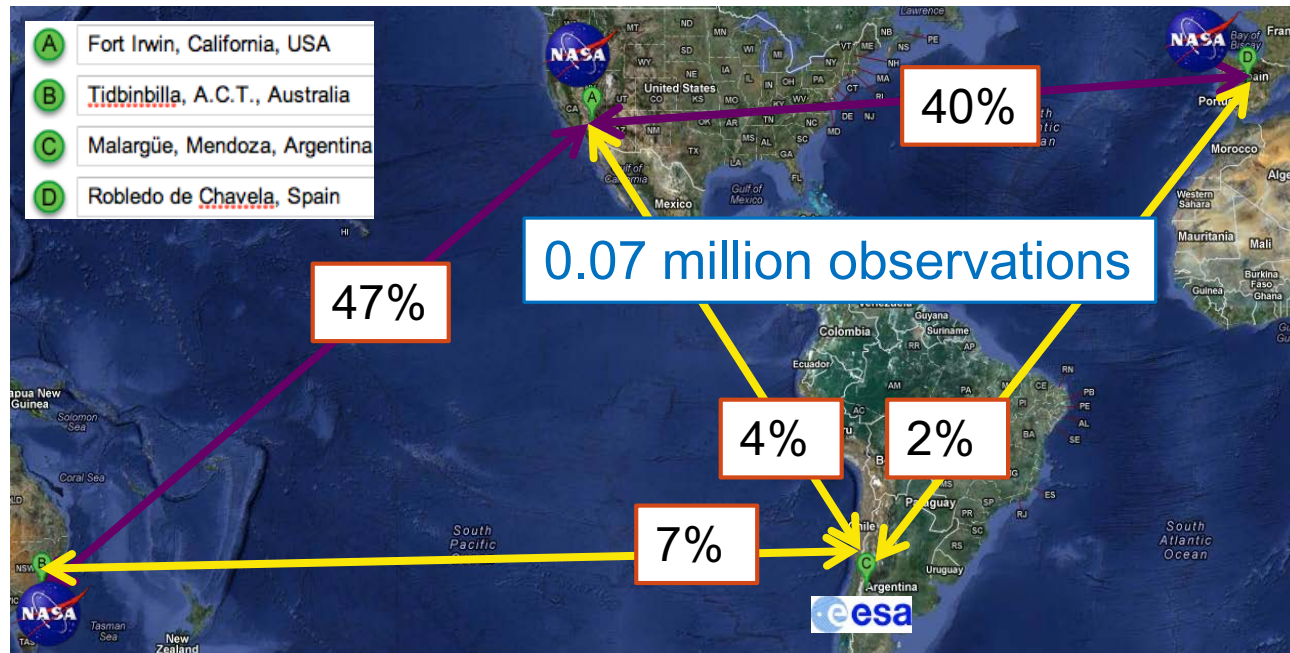


1% of data

- 40 VLBA sessions (2002-2018)
- 16 South-Africa–Australia single-baseline sessions (2014-2018)

Data sets: X/Ka band (8.4/32 GHz)

Deep Space Network + ESA antenna in Argentina

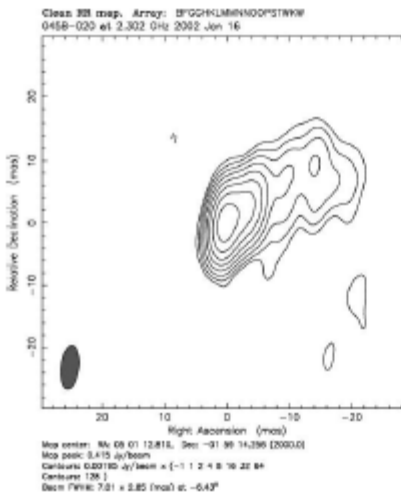


- 167 sessions using DSN antennas and occasionally (~10% of the sessions) the ESA antenna in Malargüe (2005-2018)

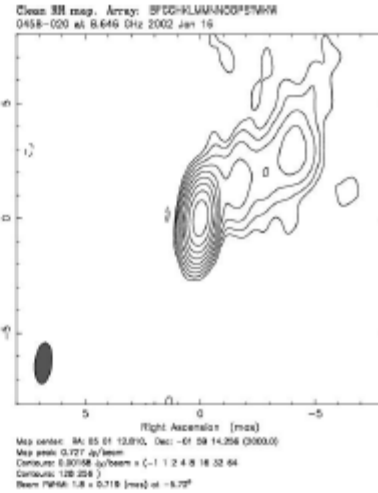
Why observing at higher frequencies ?

Evolution of source structure from 2 to 43 GHz

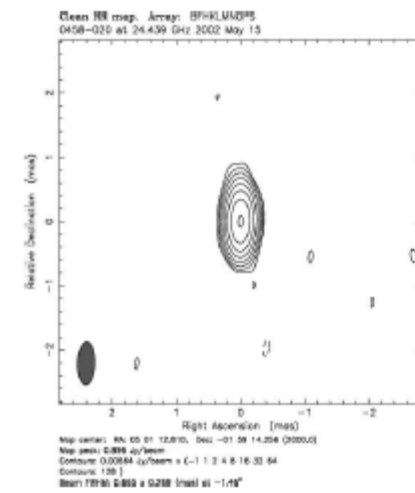
2 GHz



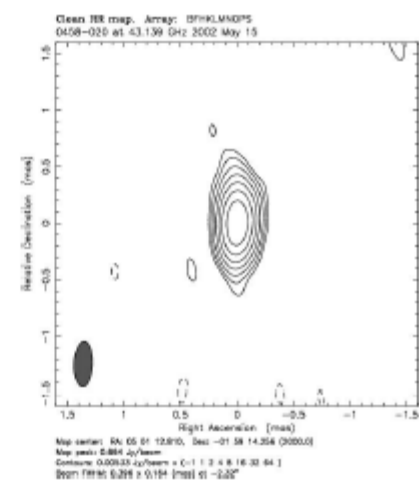
8 GHz



24 GHz



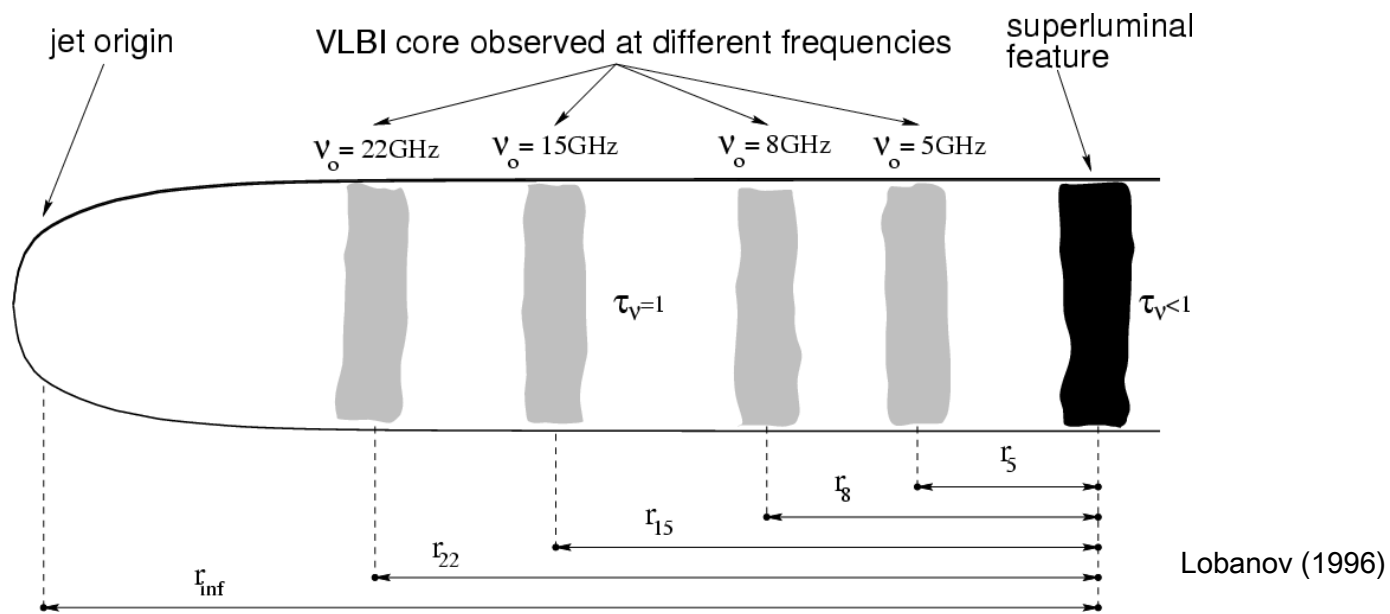
43 GHz



Credit: Radio Reference Frame Image Database

→ Source structure gets more compact at higher frequencies

Frequency-dependent jet properties

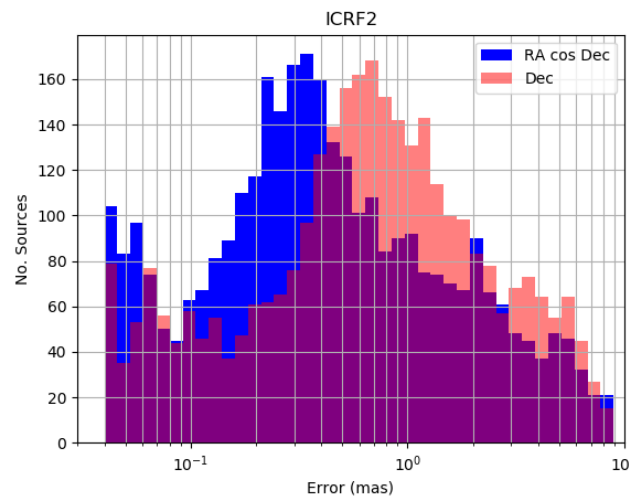
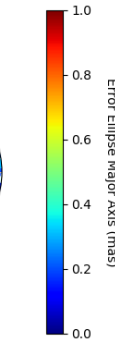
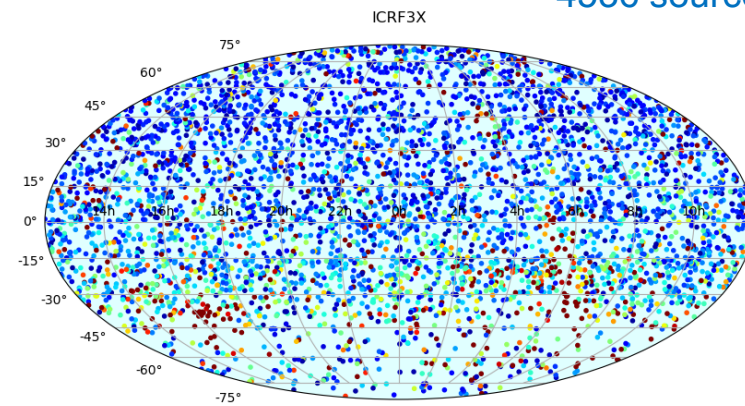
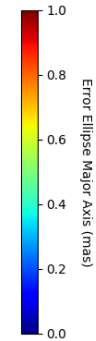
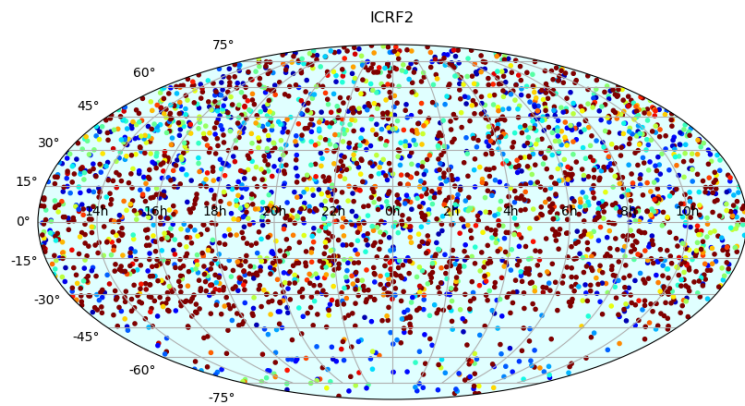


- Core emission not superimposed at different frequencies.
- Jet emission less prominent as frequency increases

Modeling and analysis configuration

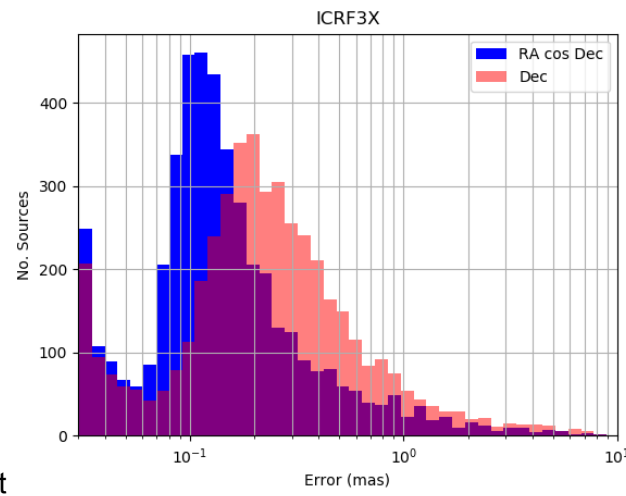
- Adhere to IERS conventions (2010)
- Ionospheric corrections (K band data) using TEC maps from GPS
- Celestial frame
 - All sources treated as global parameters
 - SX frame aligned onto ICRF2 using the 295 ICRF2 defining sources
 - K and XKa frames aligned onto SX frame using ICRF3 defining sources
- Terrestrial frame and EOP
 - Terrestrial frame aligned onto ITRF2014
 - Station coordinates treated as global parameters
 - EOP estimated per session
- Galactocentric acceleration correction of 5.8 $\mu\text{as}/\text{yr}$ applied (estimated from the SX data) – Positions given for epoch 2015.0
- Rescaling of formal position uncertainties
 - Multiplicative factor of 1.5 applied to SX and K band coordinate errors
 - 30 μas added in quadrature to α^* and δ errors (50 μas for δ at K band)

ICRF3-SX



10⁻¹ 10⁰ 10¹

Error (mas)

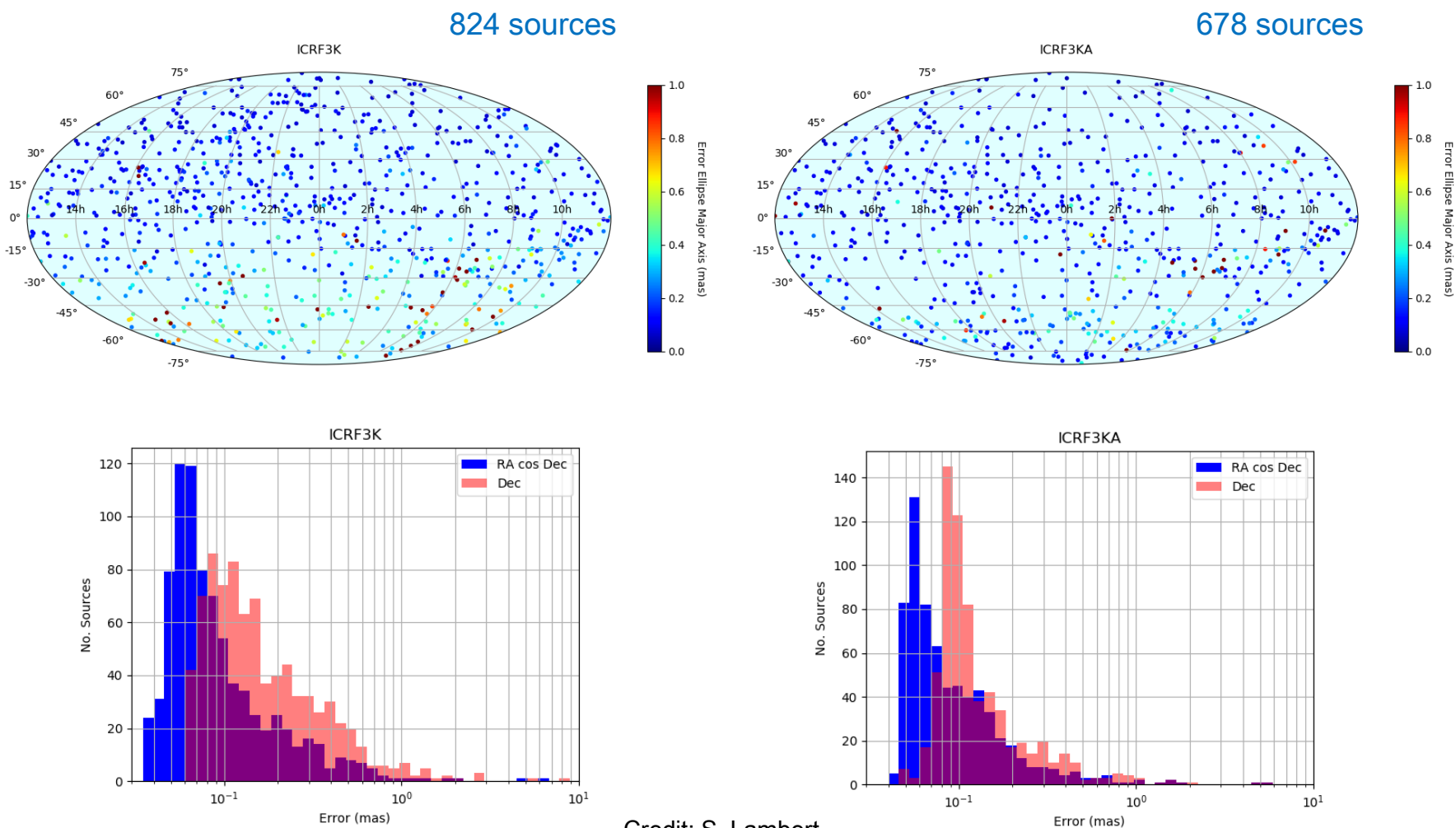


10⁻¹ 10⁰ 10¹

Error (mas)

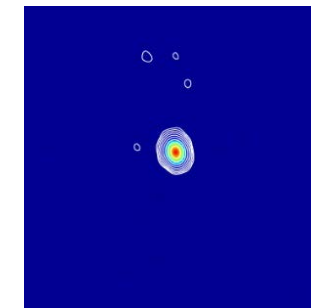
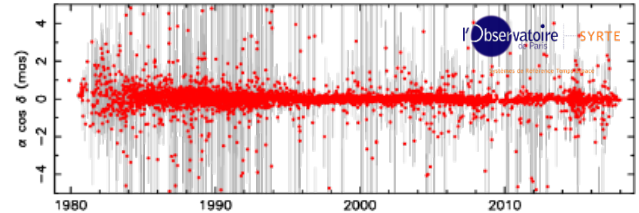
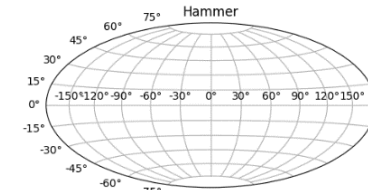
Credit: S. Lambert

ICRF3-K and ICRF3-XKa



Selection of defining sources

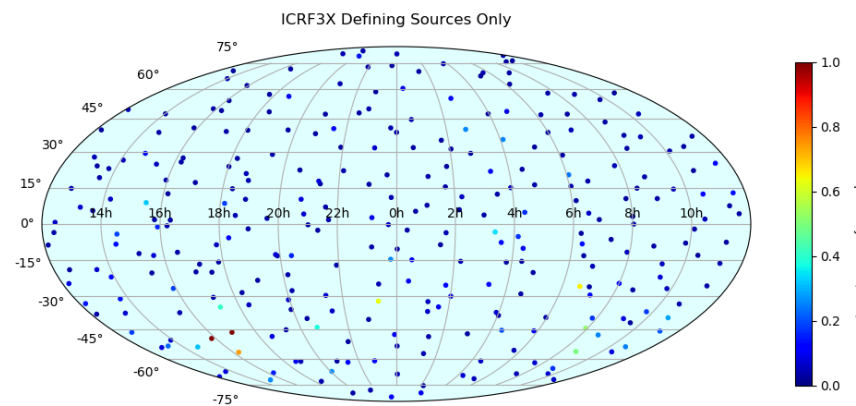
- Sub-divide the celestial sphere into 324 sectors of equal area
 - Order sources in each sector according to the quality of the position time series
 - Examine VLBI images and categorize sources depending on their structure (size, variability, structure index,...)
 - A = good or excellent
 - B = with extended structure
 - C = poor structure
- Identify the most compact and stable source in each sector and select it as defining source



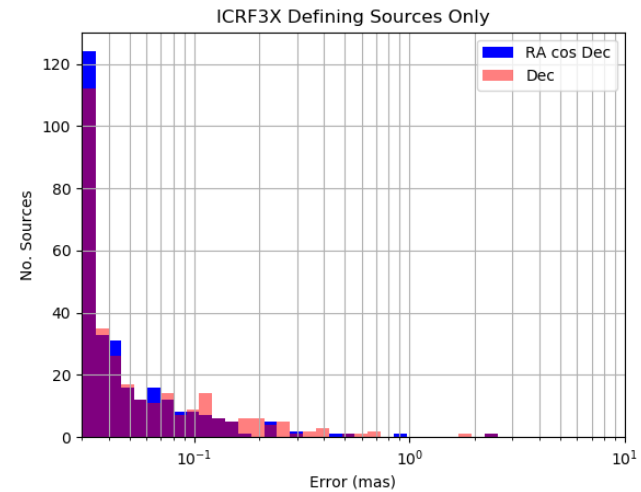
ICRF3 defining sources

- 216 sectors with a class A source 72%
- 62 sectors with a class B source 20%
- 19 sectors with only class C sources removed
- 25 sectors with structure not assessed (no images) 8%
- 2 sectors with no ICRF3 source < 1%

303 defining sources

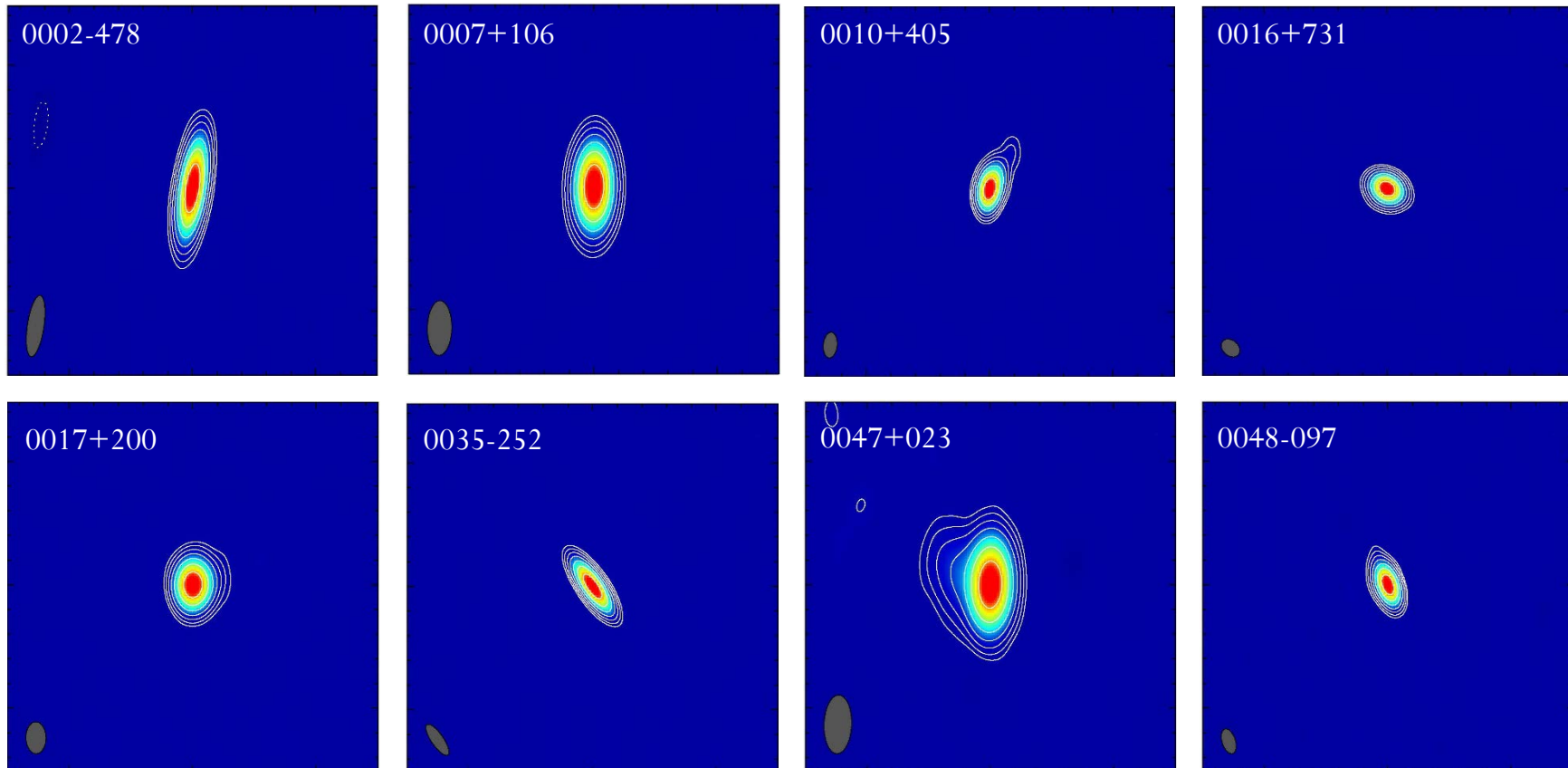


Credit: S. Lambert



Some class A defining sources

VLBI images at 8.4 GHz from the Bordeaux VLBI Image Database



Contour levels: $\pm 1, 2, 4, 8, 16, 32, 64\%$ of peak brightness

Image size: 15 x 15 mas

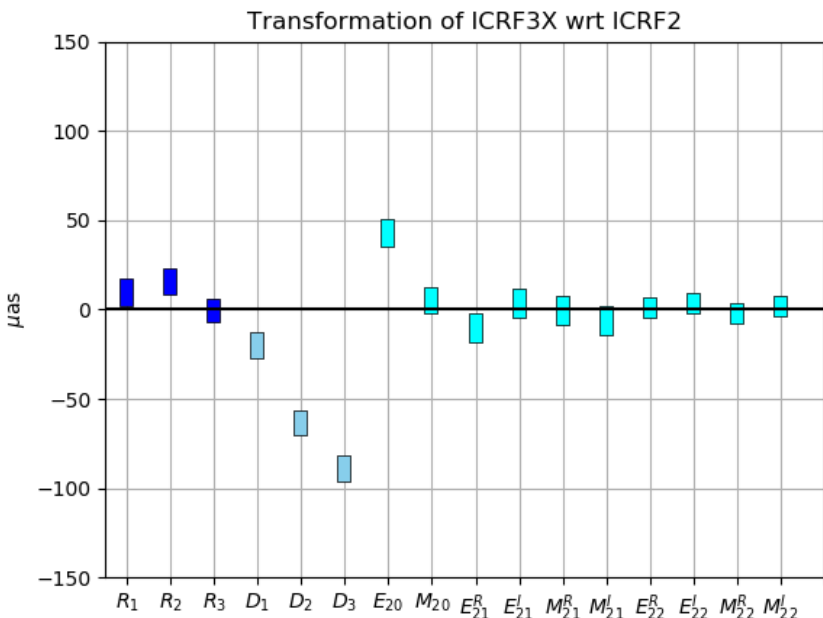
Model for comparing frames

$$\begin{aligned}\Delta\alpha \cos \delta &= R_1 \cos \alpha \sin \delta - R_2 \sin \alpha \sin \delta - R_3 \cos \delta + D_1 \sin \alpha + D_2 \cos \alpha \\ &+ a_{20}^M \sin 2\delta \\ &+ (a_{21}^{E,\text{Re}} \sin \alpha + a_{21}^{E,\text{Im}} \cos \alpha) \sin \delta \\ &- (a_{21}^{M,\text{Re}} \cos \alpha - a_{21}^{M,\text{Im}} \sin \alpha) \cos 2\delta \\ &- 2 (a_{22}^{E,\text{Re}} \sin 2\alpha + a_{22}^{E,\text{Im}} \cos 2\alpha) \cos \delta \\ &- (a_{22}^{M,\text{Re}} \cos 2\alpha - a_{22}^{M,\text{Im}} \sin 2\alpha) \sin 2\delta, \\ \Delta\delta &= -R_1 \sin \alpha + R_2 \cos \alpha - D_1 \cos \alpha \sin \delta - D_2 \sin \alpha \sin \delta + D_3 \cos \delta \\ &+ a_{20}^E \sin 2\delta \\ &- (a_{21}^{E,\text{Re}} \cos \alpha - a_{21}^{E,\text{Im}} \sin \alpha) \cos 2\delta \\ &- (a_{21}^{M,\text{Re}} \sin \alpha + a_{21}^{M,\text{Im}} \cos \alpha) \sin \delta \\ &- (a_{22}^{E,\text{Re}} \cos 2\alpha - a_{22}^{E,\text{Im}} \sin 2\alpha) \sin 2\delta \\ &+ 2 (a_{22}^{M,\text{Re}} \sin 2\alpha + a_{22}^{M,\text{Im}} \cos 2\alpha) \cos \delta\end{aligned}$$

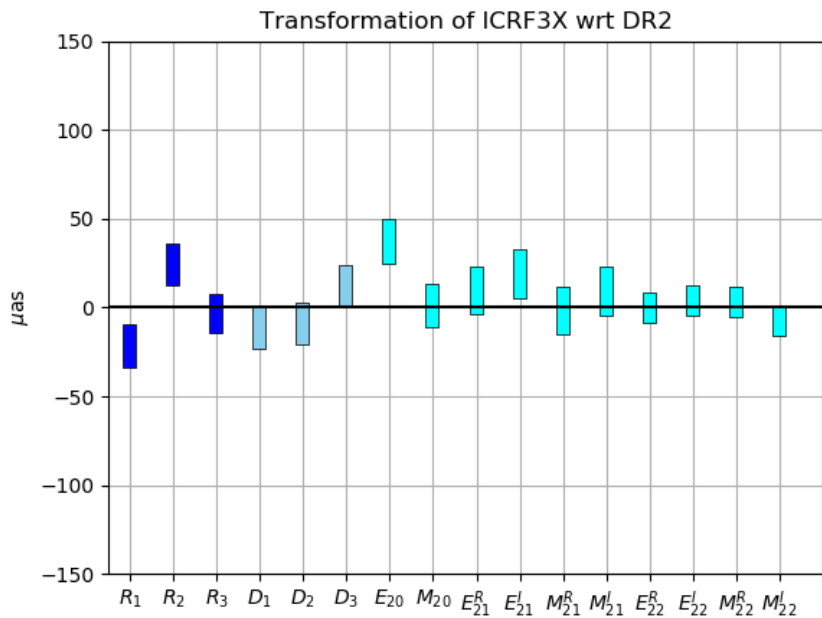
Mignard & Klioner (2012)

Deformations between frames

ICRF3-SX vs ICRF2



ICRF3-SX vs Gaia-CRF2

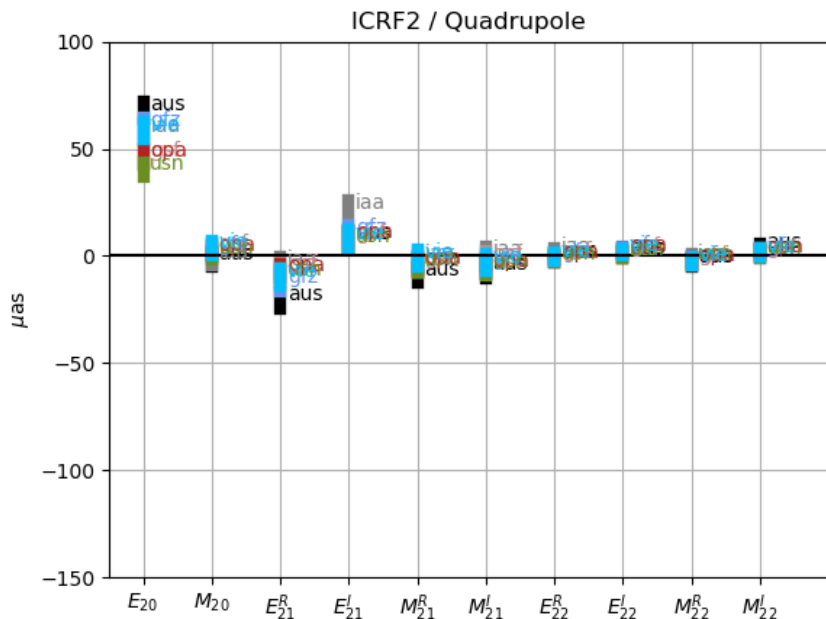
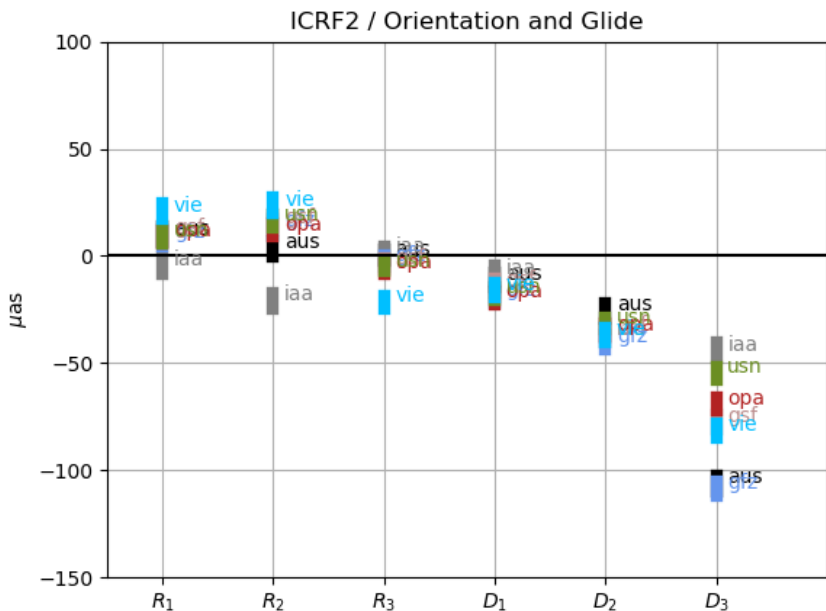


Credit: S. Lambert

- Existence of significant glide parameters D2 and D3 and quadrupole term E20 between ICRF3-SX and ICRF2
- No significant deformations between ICRF3-SX and Gaia CRF2

Deformations ICRF3-SX vs ICRF2

Impact of VLBI software packages and analyst choices

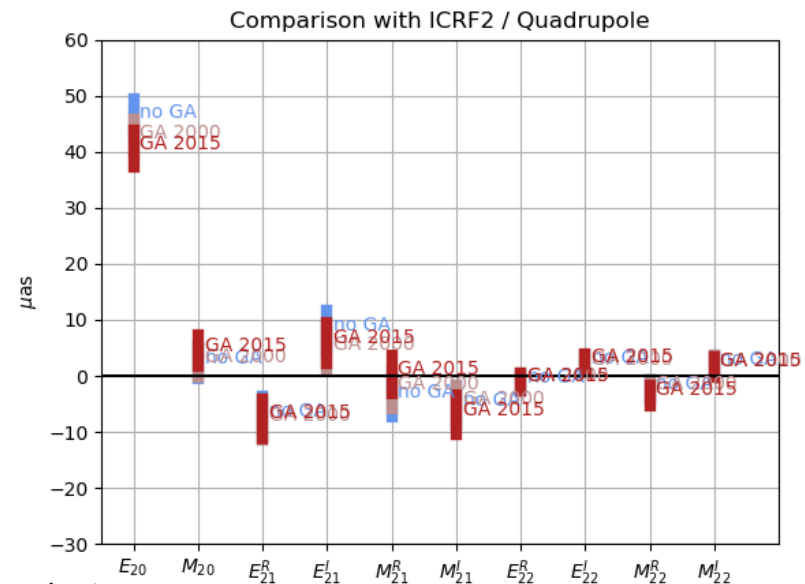
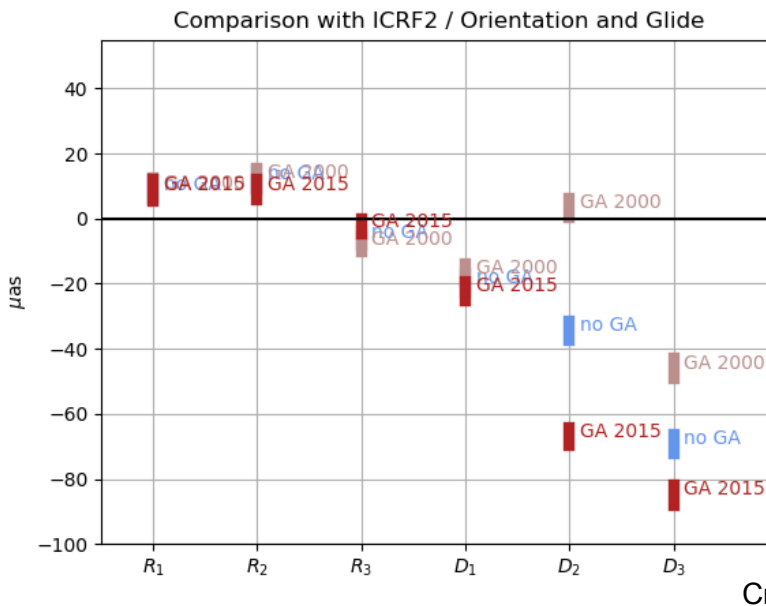


Credit: S. Lambert

- Seven ICRF3-SX variants produced from different VLBI software packages or analysts
- All show similar deformations in D2, D3 and E20.

Deformations ICRF3-SX vs ICRF2

Impact of modeling Galactocentric acceleration



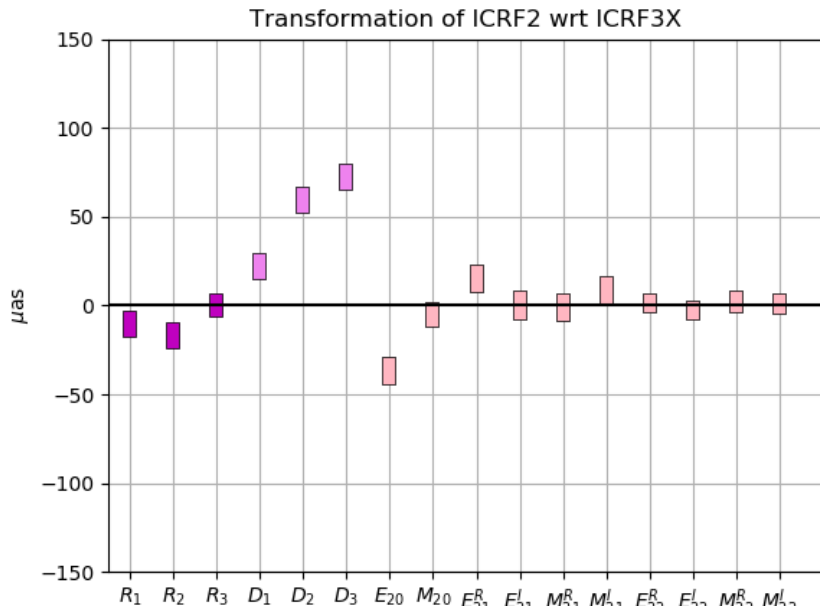
Credit: S. Lambert

- Three ICRF3-SX variants produced by changing the catalog epoch (2000.0 or 2015.0) or not incorporating Galactocentric acceleration
- Incorporation of Galactocentric acceleration or changing the catalog epoch has a significant impact on the glide parameters D2 and D3.

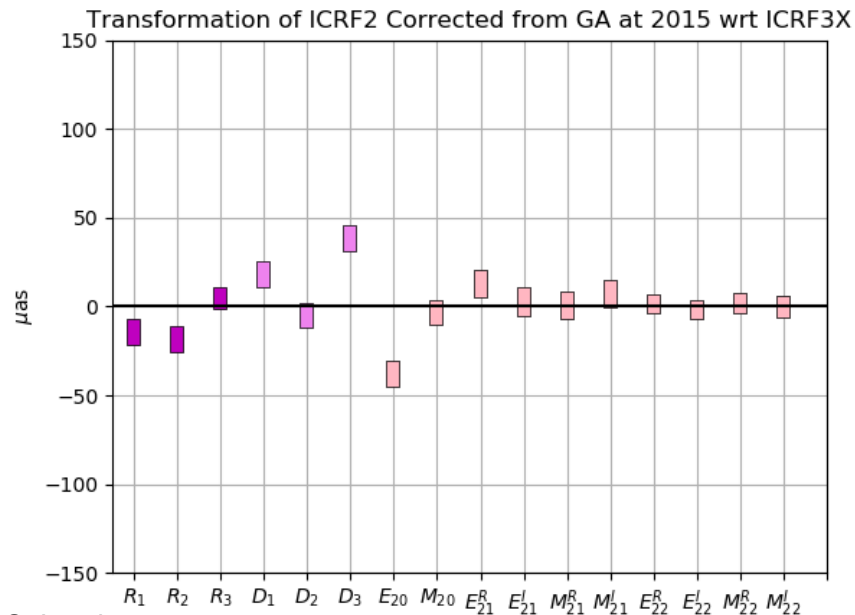
Deformations ICRF3-SX vs ICRF2

ICRF3-SX vs ICRF2 (reproduced)

ICRF3-SX vs ICRF2 (reproduced with GA modeled at epoch 2015.0)



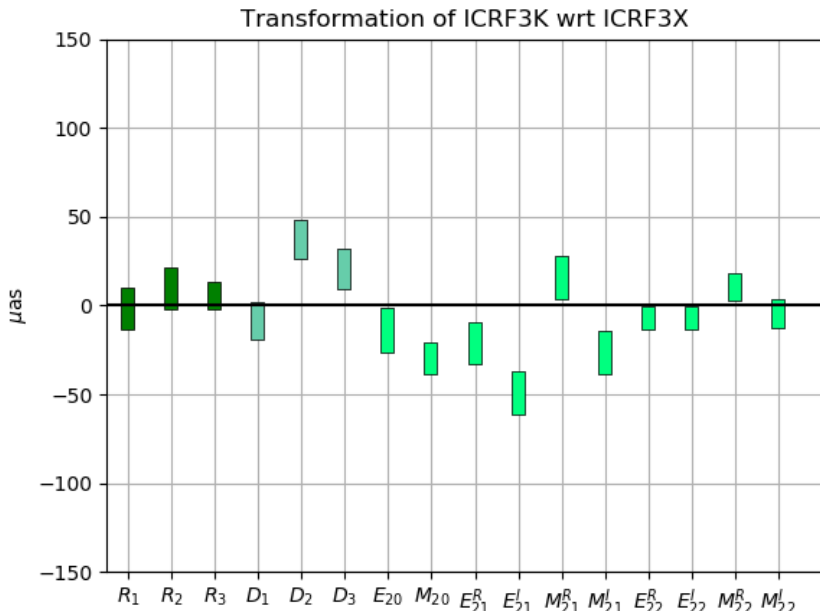
Credit: S. Lambert



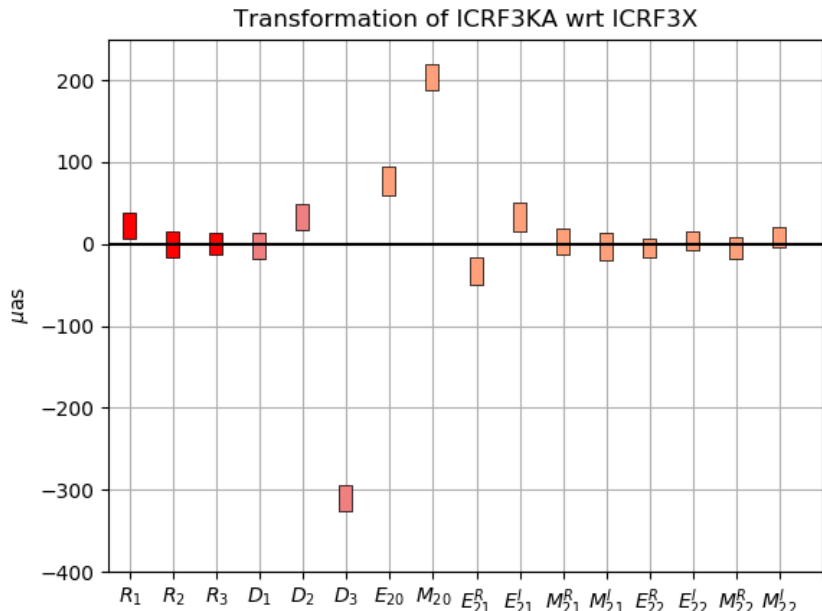
- Reproducing ICRF2 and modeling Galactocentric acceleration annihilates the D2 term and reduces the bias in D3 by 50%

Deformations: SX vs K and XKa

SX vs K



SX vs XKa



Credit: S. Lambert

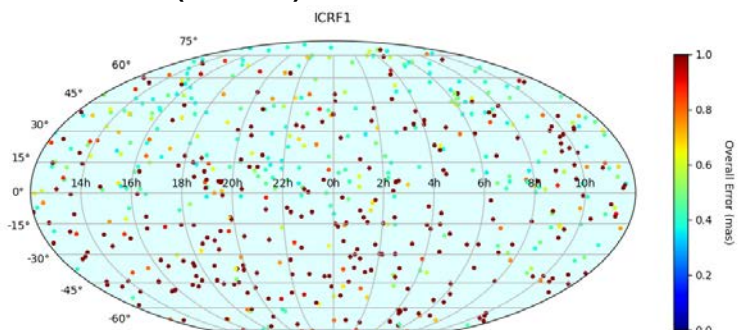
- No significant deformation between the SX band and K band frames
- Existence of significant deformation of the X/Ka frame (D3, E20, M20) originating from the limited (North-South) geometry of the network

From ICRF1... to ICRF3

	ICRF	ICRF2	ICRF3
Frequency (GHz)	8.4/2.3	8.4/2.3	8.4/2.3 / 24 / 8.4/32
Nb of observations	1.6 Million	6.5 Million	14 Million
Time range of obs.	1979-1995	1979-2009	1979-2018
Nb of sources	609	3414	4536 / 824 / 678
Nb of defining sources	212	295	303
Noise floor (μ as)	250	40	30
Adoption by IAU	1997	2009	2018

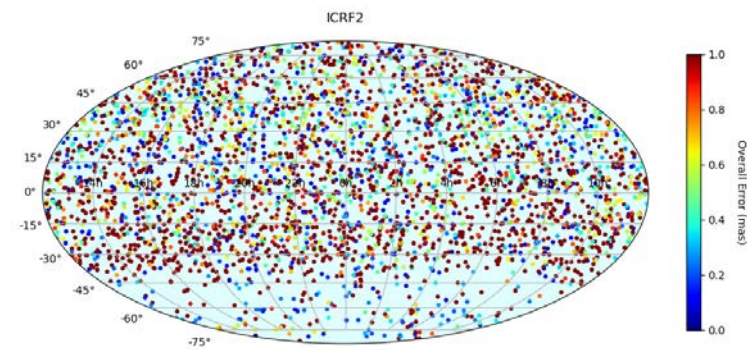
From ICRF1... to ICRF3

ICRF1 (1997)



608 sources

ICRF2 (2009)

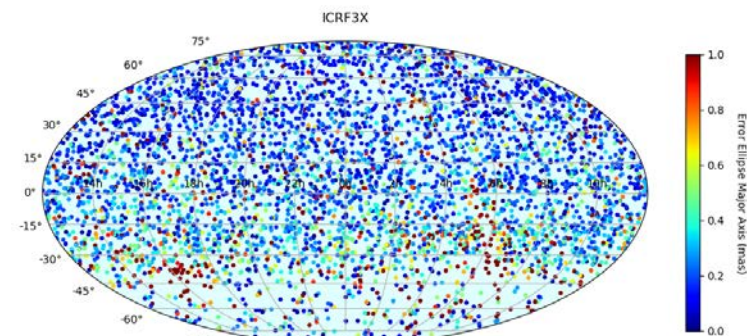


3414 sources

Main features of ICRF3

- Median position error decreased by a factor of 3.5 compared to ICRF2
- 4536 sources (1122 more than in ICRF2)
- 3-frequency positions for 600 sources
- No deformations wrt Gaia-CRF2

ICRF3 (2018)



4536 sources

Credit: S. Lambert

Adoption of ICRF3 and documentation

- ICRF3 adopted by IAU on 30 August 2018 (through resolution B2) and will replace ICRF2 on 1 January 2019
- Detailed information will be available from ICRF3 paper to be submitted in September

Astronomy & Astrophysics manuscript no. icrf3
August 29, 2018

©ESO 2018

The Third Realization of the International Celestial Reference Frame by Very Long Baseline Interferometry

P. Charlot¹, C. S. Jacobs², D. Gordon³, S. Lambert⁴, A. de Witt⁵, J. Böhm⁶, A. L. Fey⁷, R. Heinkelmann⁸, E. Skurikhina⁹, O. Titov¹⁰, E. F. Arias⁴, S. Bolotin³, G. Bourda¹, C. Ma^{3*}, Z. Malkin^{11,12}, A. Nothnagel¹³, D. Mayer⁶, D. S. MacMillan³, T. Nilsson⁸, and R. Gaume¹⁴

¹ Laboratoire d'astrophysique de Bordeaux, Univ. Bordeaux, CNRS, B18N, Allée Geoffroy Saint-Hilaire, 33615 Pessac, France
e-mail: patrick.charlot@u-bordeaux.fr

² Jet Propulsion Laboratory, California Institute of Technology, 4800 Oak Grove Drive, Pasadena, CA 91109-8099, USA

³ National Aeronautics and Space Administration, Goddard Space Flight Center, Code 698, Greenbelt, MD 20771, USA

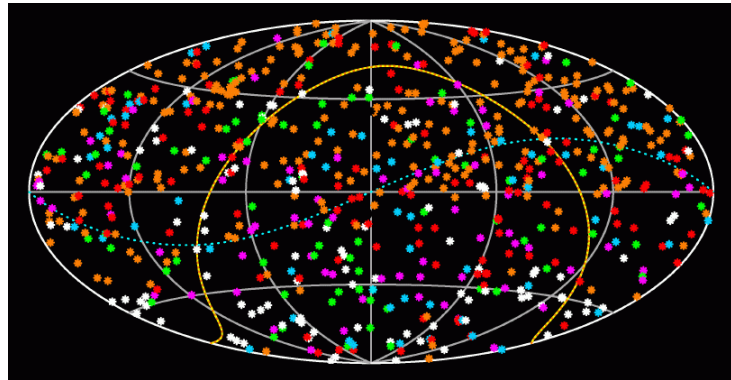
⁴ SYRTE, Observatoire de Paris, Université PSL, CNRS, Sorbonne Université, LNE, 61 Avenue de l'Observatoire, 75014 Paris, France

⁵ Hartebeesthoek Radio Observatory, PO Box 443, Krugersdorp 1740, South Africa

⁶ Department of Geodesy and Geoinformation, Technische Universität Wien, Karlsplatz 13, 1040 Vienna, Austria

Applications of the ICRF

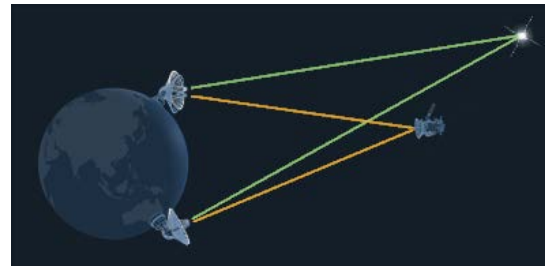
Spacecraft navigation



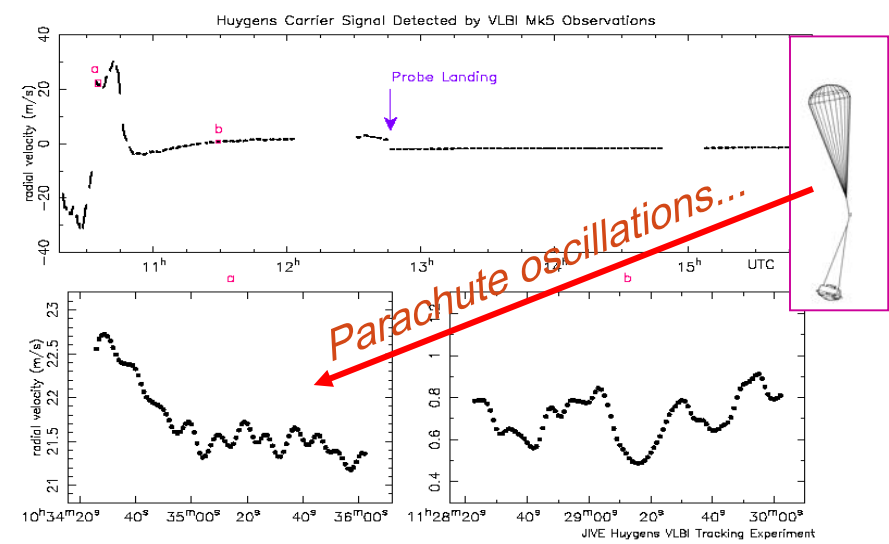
Credit:
ESA – D.
Ducros

Descent of Huyguens in the atmosphere of Titan tracked with VLBI to 1 km level

VLBI differential observations with respect to a nearby angularly-close quasar



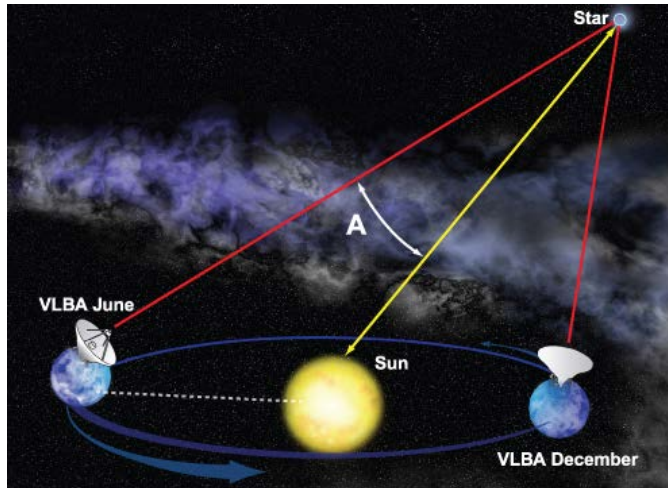
Credit: NASA



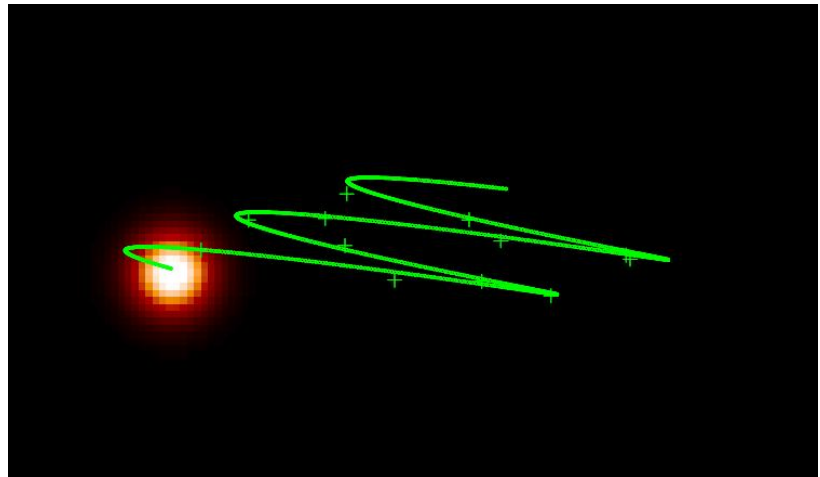
Credit: L. Gurvits

Distances and proper motions in the Galaxy

Annual parallax



Apparent displacement on the sky

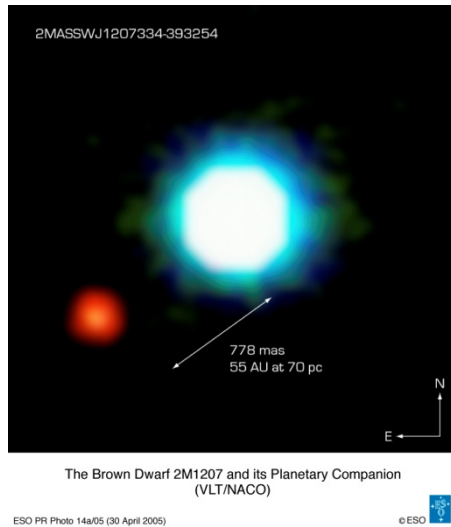


Credit: Bill Saxton, NRAO / AUI / NSF

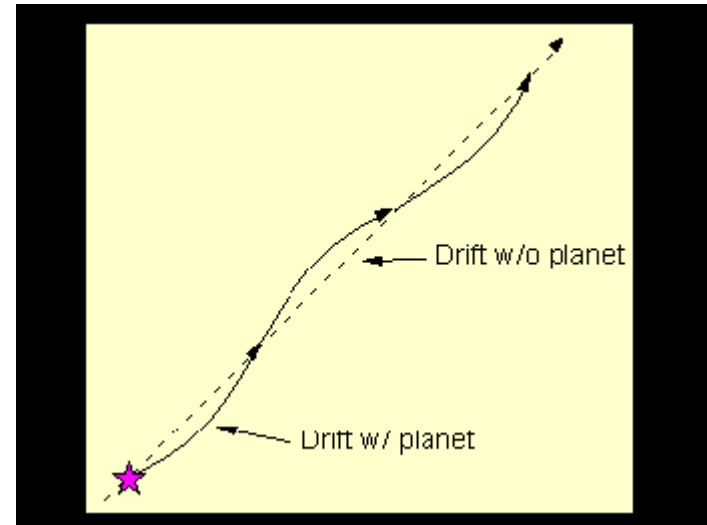
- Differential VLBI observations with respect to a nearby angularly-close quasar
- Example: determination of the distance of the Taurus star forming regions to 1% (Loinard et al. 2007).
→ Only known to 15% before (from Hipparcos data)

Detection of extrasolar planets ?

Star + planet



Perturbation of the star motion due to the presence of the planet

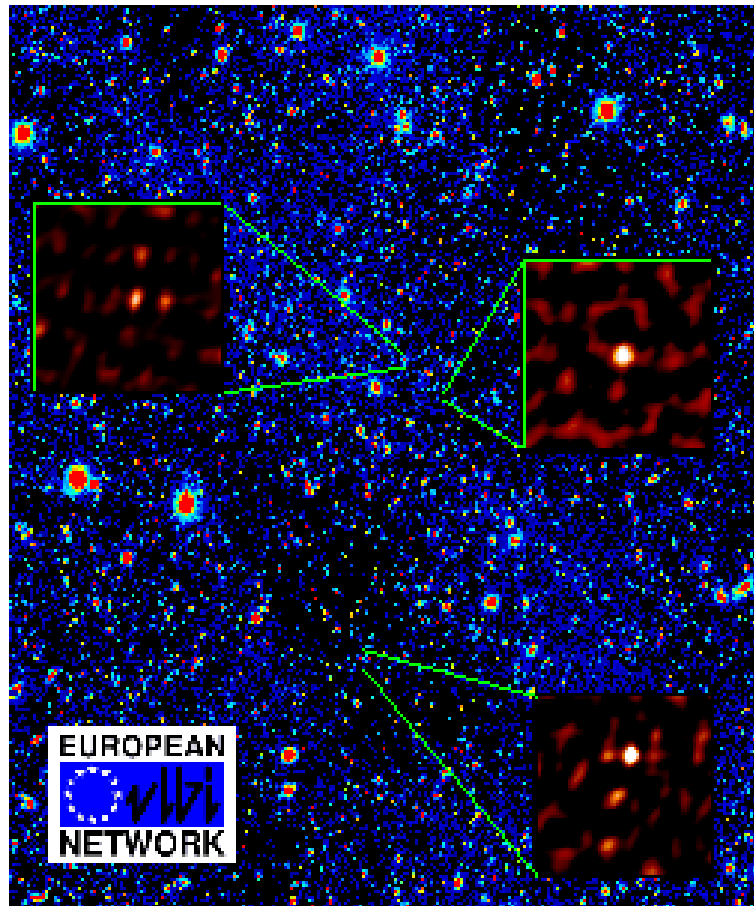


- Differential VLBI observations with respect to a nearby angularly-close quasar
- Requires $< 100 \mu\text{as}$ accuracy on the individual astrometric positions of the star over time

Observations of very weak objects

- Use the VLBI phase-referencing technique
 - Permits « integration » on a source for several hours (instead a few minutes with standard mode)
 - Needs angular-close quasar
- Observations of the Hubble Deep Field (HDF) with the EVN
 - Detection of 3 very weak radio sources ($\sim 200 \mu\text{Jy}$)
 - More than 100 times weaker than the weakest sources in ICRF

Hubble Deep Field (HDF) vu par l'EVN

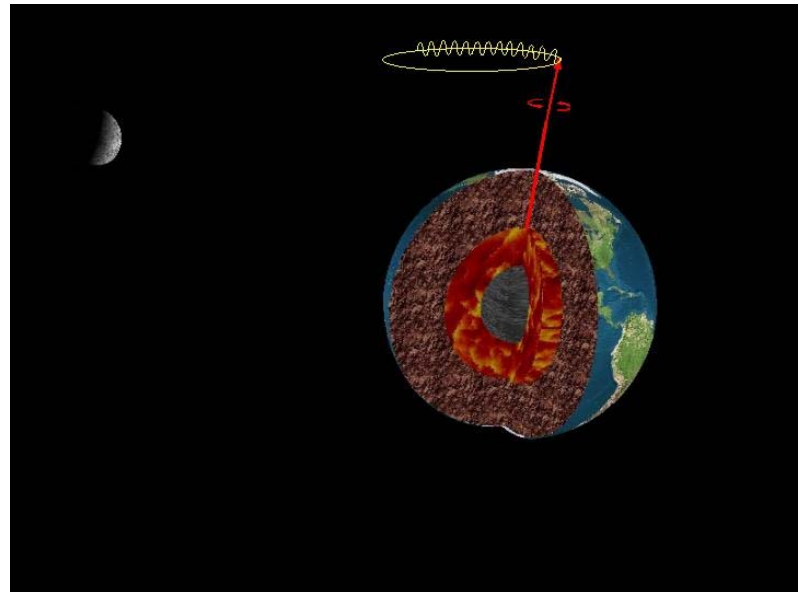


Credit: M. Garrett

The Earth's orientation

- Precession and nutation are caused by the gravitational attraction of the Sun and Moon
- The Earth's response depends on its constitution (in particular on the geometry of the core)

Motion in space of the axis of rotation of the Earth

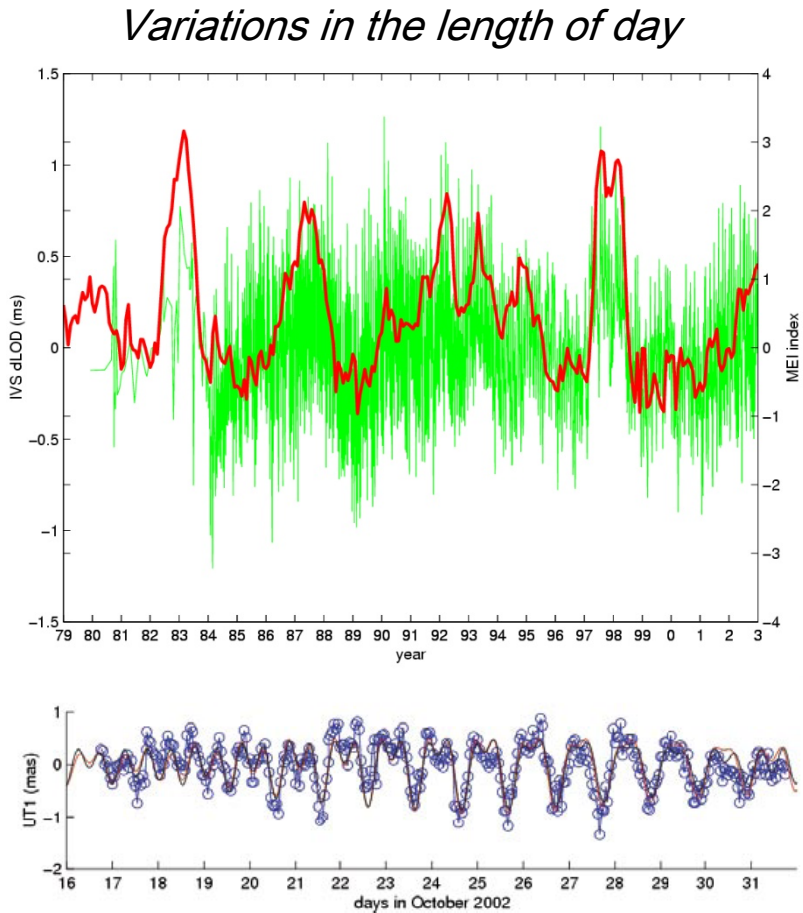


Credit: IVS

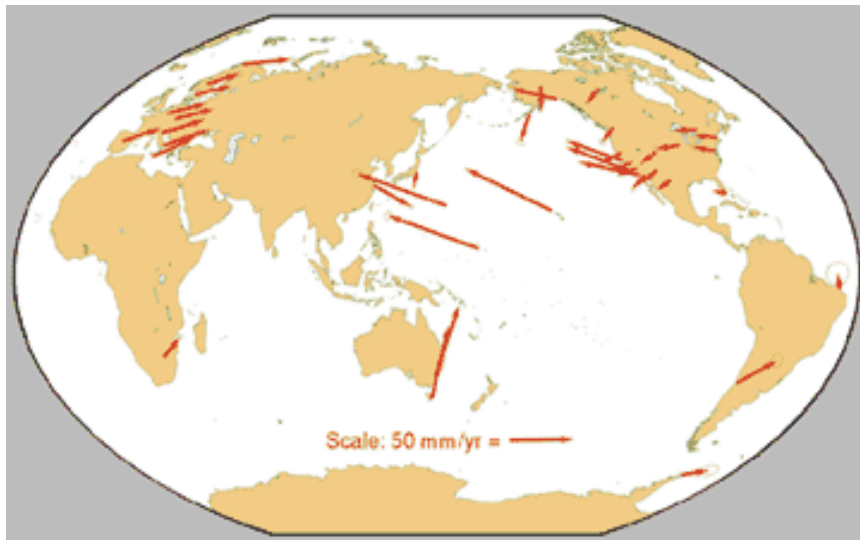
- Ultra-precise monitoring of the Earth's precession and nutation with respect to distant quasars (using VLBI) allows one to learn about the Earth's interior

The Earth's rotation

- The length of day (LOD) varied by about 2 milliseconds over 20 years
- Mid- to long-term variations in the LOD (from one week to several years) originate mostly from changes in the atmosphere.
- Short-term variations (from a few hours to a few days) come mostly from oceanic tides



Crustal deformations on the Earth surface

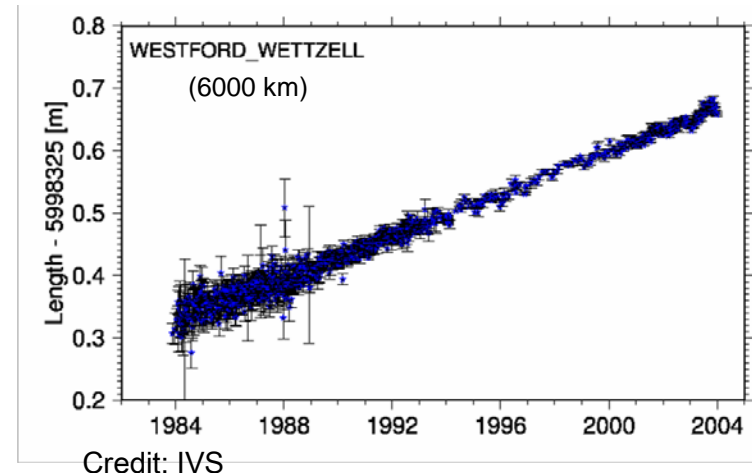


Credit: NASA/GSFC

Tectonic plate motions
directly measured by
VLBI

Increase in the distance
between Europe and USA

30 cm in 20 years



Credit: IVS

Thank you for your attention

